BIOCHEMISTRY
including biophysical chemistry & molecular biology

Article

pubs.acs.org/biochemistry

Protein Engineering of the N-Terminus of NEMO: Structure Stabilization and Rescue of IKKβ Binding

Bingqian Guo,[†] Christopher O. Audu,[‡] Jared C. Cochran,[§] Dale F. Mierke,[†] and Maria Pellegrini*[,†]

[†]Department of Chemistry, Dartmouth College, Hanover, New Hampshire 03755, United States
[‡]The Geisel School of Medicine, Dartmouth College, Hanover, New Hampshire 03755, United States
[§]Molecular and Cellular Biochemistry Department, Indiana University, Bloomington, Indiana 47405, United States

Supporting Information

ABSTRACT: NEMO is a scaffolding protein that, together with the catalytic subunits IKKα and IKKβ, plays an essential role in the formation of the IKK complex and in the activation of the canonical NF-κB pathway. Rational drug design targeting the IKK-binding site on NEMO would benefit from structural insight, but to date, the determination of the structure of unliganded NEMO has been hindered by protein size and conformational heterogeneity. Here we show how the utilization of a homodimeric coiled-coil adaptor sequence stabilizes the minimal IKK-binding domain NEMO(44−111) and furthers our understanding of the structural requirements for IKK binding. The engineered constructs incorporating the coiled coil at the N-terminus, C-terminus, or both ends of NEMO(44−111) present high thermal stability and cooperative melting and, most importantly, restore IKKβ binding affinity. We examined the consequences of structural content and stability by circular dichoism and nuclear magnetic resonance (NMR) and measured the binding affinity of each construct for IKKβ(701−745) in a fluorescence anisotropy binding assay, allowing us to correlate structural characteristics and stability to binding affinity. Our results provide a method for engineering short stable NEMO constructs to be suitable for structural characterization by NMR or X-ray crystallography. Meanwhile, the rescuing of the binding affinity implies that a preordered IKK-binding region of NEMO is compatible with IKK binding, and the conformational heterogeneity observed in NEMO(44−111) may be an artifact of the truncation.

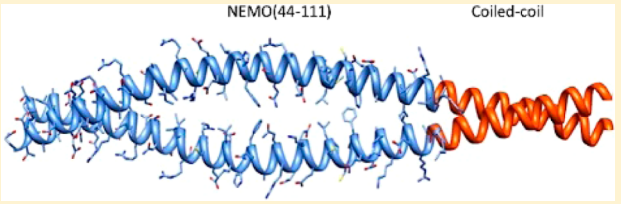

The nuclear factor κB (NF-κB) essential modulator, NEMO (also known as IKKγ), is a scaffolding protein that together with the catalytic subunits IKKα (inhibitor of κ B kinase α) and IKKβ forms the IKK complex, a central node in the canonical NF-κB pathway.[1] The NF-κB pathway regulates the expression of a large number of genes responsible for immune response, inflammation, cell proliferation and survival, and cancer and, as such, is considered an attractive target for new therapies.[2−6] Upon activation by a variety of stimuli, the IKK complex phosphorylates the inhibitor of κB molecules (IκB), responsible for keeping NF-κB sequestered in the cytoplasm. IκB is then ubiquitinated and degraded by the ubiquitin−proteasome system, freeing NF-κB to enter the nucleus and activate target genes.[7,8] Pharmacological inhibition of the NF-κB pathway has been proposed and attempted at many different levels (reviewed in ref 9), including targeting the IKK-binding domain of NEMO. Some success was reported in the utilization of a six-amino acid peptide encompassing the sequence found at the C-terminus of both IKKα and IKKβ, the NEMO-binding domain [L^{737}DWSWL^{742} (NBD)], which binds to NEMO and effectively interferes with the formation of the IKK complex.[12,13] A cell-permeable NBD peptide was demonstrated to be an effective blocker of acute and chronic inflammatory signaling in models of inflammation and to be effective in models of cancer.[14−19]

We previously reported the structure of dimeric NEMO(44−111) in complex with a longer fragment of IKKβ(701−745) (Figure 1A).[20] As for most protein−protein interaction interfaces, the NEMO−IKKβ interface is extended and prevalently flat and possibly difficult to target with small molecule inhibitors,[10,11] but rational inhibitor design would greatly benefit from the knowledge of the structure of unliganded NEMO or NEMO in the presence of small molecule ligands. NEMO constructs of any length encompassing the IKKβ-binding domain have never been crystallized in the apo form and produce nuclear magnetic resonance (NMR) spectra of poor quality.[20] NEMO(44−111) in particular, the minimal IKK-binding domain, is characterized in our hands by conformational heterogeneity and reduced thermal stability and binding affinity, making unlikely a successful determination of the structure. Structure prediction indicates a helical sequence (residues 49−94) followed by a coiled-coil region (103−130),[20] although experimental confirmation of a dimeric structure for unliganded NEMO(44−111) was not reported. While unliganded NEMO(44−111) is characterized by structural instability, upon binding IKKβ it undergoes a

Received: July 11, 2014
Revised: September 25, 2014
Published: October 6, 2014

   dx.doi.org/10.1021/bi500861x | *Biochemistry* 2014, 53, 6776−6785

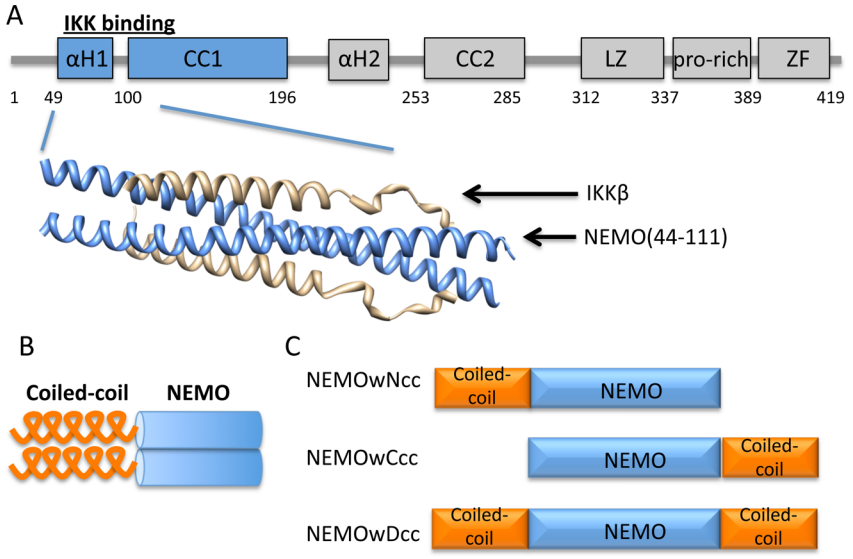

Figure 1. (A) Domain structure of full length NEMO and X-ray structure of NEMO(44−111) in complex with IKKβ(701−745) (Protein Data Bank entry 3BRV). αH regions are the helical regions. CC1 and CC2 are the first and second coiled-coil regions, respectively. LZ is the leucine zipper region. ZF is the zinc finger domain. (B) Concept of using a coiled-coil adaptor to stabilize the NEMO dimer. (C) Engineered coiled-coil NEMO constructs.

conformational change and locks into a stable structure, but it remains unclear whether the conformational heterogeneity of the short construct is an artifact of construct truncation or an intrinsic characteristic of this portion of NEMO required for IKKβ binding.

Here we report the design and characterization of a series of constructs encompassing the IKK-binding domain of NEMO that we engineered to achieve improved stability and structural homogeneity and to assess the effect of this stabilization on binding affinity. The NEMO(44−111) constructs incorporate an ideal coiled-coil sequence based on GCN4 at the N-terminus, C-terminus, or both termini (Figure 1B,C).[21,22] The coiled-coil extension was chosen to stabilize the hypothesized dimeric structure of NEMO and possibly nucleate coiled-coil zipping. Our study shows that the coiled-coil adaptor indeed increases the stability of the short NEMO constructs and restores their IKKβ binding affinity. Finally, we show that the stabilized construct with a C-terminal coiled-coil adaptor is able to recognize and bind endogenous IKKβ in mammalian cells.

EXPERIMENTAL PROCEDURES

Chemicals. Ampicillin (Sigma), isopropyl β-D-1-thiogalactopyranoside (IPTG) (Amresco), Tris base (Fisher Scientific), glycerol (Invitrogen), magnesium chloride (Fisher Scientific), imidazole (Sigma), benzonase (Sigma), NP40, urea (Fisher Scientific), sodium chloride (Fisher Scientific), dithiothreitol (DTT) (Soltec Venture), 5-carboxyfluorescein (5′FAM) (Nova Biochem), *N*-hydroxysuccinimide (NHS), and dimethyl sulfoxide (DMSO) (Acros) were acquired and used.

Protein Expression and Purification. A list of primers utilized in the cloning is reported in Table S1 of the Supporting Information. The NEMO(1−196) construct was cloned into a pGEX-6P-1 vector with an N-terminal GST tag.

The procedure used for protein production was as described previously[20] with the following exceptions: induction with 0.2 mM IPTG, purification by affinity chromatography with a GSTrap 4B column [GE Healthcare, washing with 50 mM Tris (pH 8), 150 mM NaCl, 5 mM DTT, and 1 mM EDTA; elution with 50 mM Tris (pH 8), 150 mM NaCl, 5 mM DTT, 1 mM EDTA, and 10 mM reduced glutathione] followed by size exclusion chromatography (SEC) [50 mM sodium phosphate (pH 6.5), 150 mM NaCl, and 5 mM DTT] on a Superdex75 16/60 column (GE Healthcare Life Sciences). All the denaturing steps utilized 8 M urea.

The NEMO(44−111) construct was cloned into a pET-16b vector with a TEV cleavage site inserted before the NEMO sequence. A tryptophan was inserted at the N-terminus of the NEMO construct for UV detection. The final construct has residues GSW before the NEMO sequence as a result of the TEV cleavage and W insertion and is termed NEMOw. The vector was transformed into BL21 Star (DE3) cells for protein production. A 250 mL culture was induced with 0.2 mM IPTG at 20 °C overnight. Cell pellets were collected after centrifugation at 4000 rpm for 30 min at 4 °C and resuspended in 25 mL of lysis buffer [50 mM Tris (pH 8), 200 mM NaCl, 10 mM imidazole, 5 mM $MgCl_2$, 0.02% NP40, 5% glycerol, one tablet of Roche protease inhibitor, and 3 μL of benzonase]. A French press was used to lyse cells, and the lysate was denatured by adding 8 M urea. The urea lysate was centrifuged at 40000 rpm for 30 min at 25 °C after being shaken overnight at room temperature. The supernatant was applied to a HisTrap 5 mL FF column (GE Healthcare Life Sciences) for purification and on-column refolding. After elution with buffer [50 mM Tris (pH 8), 200 mM NaCl, 500 mM imidazole, and 2 mM DTT], Bradford reagent was used to determine the protein concentration. Subsequently, His-tagged TEV protease was added at a ratio of 1 mg of TEV to 10 mg of His-tagged protein for TEV cleavage in dialysis buffer [25 mM Tris (pH 8), 100 mM NaCl, and 2 mM DTT] overnight at 4 °C. The cleavage mixture was applied to the HisTrap column again to remove the His tag and TEV, while the untagged protein in the flow-through was collected and concentrated to 5 mL for SEC with a Superdex75 16/60 column in 20 mM Tris (pH 8), 100 mM NaCl, and 2 mM DTT.

All other NEMO constructs were derived from the NEMOw construct using site-directed mutagenesis (QuikChange XL II

dx.doi.org/10.1021/bi500861x | *Biochemistry* 2014, 53, 6776−6785

mutagenesis kit) and expressed and purified in the same manner. The DNA for the coiled-coil sequence was amplified by polymerase chain reaction from DNA received as a kind gift from D. Bolon (University of Massachusetts Medical School, Worcester, MA). [^{15}N]NEMOw and [^{15}N]NEMOwCcc8aa were expressed and purified like the unlabeled version, utilizing M9 minimal medium supplemented with 3 g/L $^{15}NH_4Cl$ (CIL) for cell growth.[23]

The IKKβ(701−745) construct was cloned into an engineered pJCC04a vector as previously described, with a thioredoxin fusion protein and a TEV cleavage site.[23] It was purified in the same fashion as NEMO(44−111) with denaturing and on-column refolding followed by TEV cleavage and finally SEC. The K703R, K704R double-lysine mutant (IKK$\beta_{KK/RR}$) was generated using site-directed mutagenesis (QuikChange Lightening site-directed mutagenesis kit) and purified following the same procedure, but using a different SEC buffer [100 mM sodium phosphate (pH 9.3), 100 mM NaCl, and 2 mM DTT].

The protein concentration was determined by measuring the UV absorbance at 280 nm, and the extinction coefficients were obtained using the ProtParam tool from the ExPASy Server.[24]

Sodium Dodecyl Sulfate−Polyacrylamide Gel Electrophoresis (SDS−PAGE). Each of the purified samples was prepared for SDS−PAGE with 5× SDS sample loading buffer, and either with or without 200 mM DTT. Samples were heated at different temperatures, either 95 or 60 °C, for 10 min. Electrophoresis was conducted in 12% polyacrylamide gels following standard protocols (Life Technologies). Protein bands were visualized using Coomassie blue G-250 (Amresco) stain.

Fluorescent Labeling of IKK$\beta_{KK/RR}$. 5′FAM fluorescein was activated by being mixed with NHS and EDC at a 1:1:1 ratio in DMSO and then incubated at room temperature for 20 min to activate 5′FAM. Purified IKK$\beta_{KK/RR}$ was concentrated to ∼2 mg/mL, and a 10-fold molar ratio of the 5′FAM-NHS was added to 500 μL of IKK$\beta_{KK/RR}$. The mixture was left slowly swirling in the dark for 30 h at 4 °C. Labeled IKK$\beta_{KK/RR}$ was loaded on a Superdex75 10/300GL column to separate excess fluorescein in 1× phosphate-buffered saline (PBS). The concentration of 5′FAM-IKKβ was measured as previously described.[25]

Size Exclusion Chromatography (SEC) Binding Assay. A Superdex75 10/300GL column was used to confirm the binding of 5′FAM-IKK$\beta_{KK/RR}$ with NEMO. A sample of 5′FAM-IKK$\beta_{KK/RR}$ with NEMO(44−111) was prepared by mixing the two components at a 1:1 molar ratio and incubating on ice for 3 h. A 500 μL aliquot of the mixture was then injected onto the column and compared with the chromatogram of 500 μL of purified 5′FAM-IKK$\beta_{KK/RR}$ alone. Detection utilized wavelengths of 280 and 495 nm (characteristic absorption wavelength of 5′FAM).

Circular Dichroism (CD) Spectroscopy. Different NEMO constructs were prepared in Tris buffer [20 mM Tris (pH 8), 100 mM NaCl, and 2 mM DTT] with concentrations ranging from 10 to 20 μM. CD spectra were acquired from 200 to 250 nm at 20 °C (Jasco J-185) using a 0.1 cm cuvette. Melting curves were obtained by recording the ellipticity at 222 nm from 10 to 90 °C with a temperature gradient of 1 °C/min. The mean residue ellipticity was calculated using the equation[26]

$$[\theta] = (100\theta)/(nlC)$$

where $[\theta]$ is the mean residue ellipticity, θ is the measured ellipticity in millidegrees, l is the path length of the sample cell in centimeters, C is the concentration of the protein in millimolar units, and n is the number of residues. The α-helical content was calculated with the K2D3 method.[27,28]

Fluorescence Anisotropy (FA) Assay. Direct binding measurements were taken at a constant concentration of the reporter peptide 5′FAM-IKK$\beta_{KK/RR}$ (30 nM) and protein concentrations that ranged from micromolar to nanomolar, as described previously.[29] Fluorescence anisotropy was determined using a Tecan F500 Infinite plate reader, an excitation wavelength of 485 nm, and an emission wavelength of 525 nm as[25]

$$r = 1000(I_{\parallel} - I_{\perp})/(I_{\parallel} + 2I_{\perp})$$

Data were fit to a modified quadratic binding equation by nonlinear regression analysis using KaleidaGraph:[30,31]

$$Y = m_1 + (m_2 - m_1)[[L] + K_D + [R] - \sqrt{([L] + K_D + [R])^2 - 4[L][R]}]/2[L]$$

where m_1 is the anisotropy of the reporter peptide in the absence of NEMO, m_2 is the anisotropy value when all 5′FAM-IKK$\beta_{KK/RR}$ is bound to NEMO, and [L] and [R] are the total concentrations of the ligand (5′FAM-IKKβ) and receptor (NEMO), respectively.

Competition binding experiments were performed as previously described.[29] IC_{50} values were obtained by fitting the data to the following sigmoidal dose−response curve equation using KaleidaGraph.

$$Y = m_1 + (m_2 - m_1)/[1 + (x/m_3)^{m_4}]$$

where m_1 and m_2 are the anisotropy values at highest and zero inhibitor concentrations, respectively, m_3 is the log(IC_{50}) value, and m_4 is the slope factor.

K_i was calculated according to its relationship with IC_{50} as follows:[32]

$$K_i = IC_{50}/(1 + [L]/K_D)$$

where IC_{50} and K_D were obtained from the equations presented above and [L] is the total concentration of the ligand.

NMR Spectroscopy. Samples for NMR contained 96 μM [^{15}N]NEMOw or 73 μM [^{15}N]NEMOwCcc8aa and 145 or 107 μM unlabeled IKKβ(701−745), respectively (1:1.5 NEMO:IKKβ ratio), in 25 mM phosphate buffer (pH 6.5), 100 mM NaCl, and 5% D_2O. All NMR data were acquired on a 700 MHz Bruker Avance III spectrometer equipped with a TCI cryogenic probe, at 308 K. ^{1}H−^{15}N TROSY spectra were acquired with 2048 × 128 points in 128 scans.[33−35] Data were multiplied by a squared cosine bell or Gaussian function prior to Fourier transformation. Data analysis utilized Topspin 3.2 (Bruker Biospin). Molecular graphics images were produced using the UCSF Chimera package from the Computer Graphics Laboratory, University of California, San Francisco (supported by National Institutes of Health Grant P41 RR-01081).

Co-Immunoprecipitation. We cloned the NEMOwCcc construct into the pCDNA3.1 vector, incorporating an N-terminal FLAG tag for co-immunoprecipitation (co-IP) experiments. HEK293 cells were plated at a density of 10^6 cells/well in six-well plates in 2 mL of Dulbecco's modified Eagle's medium with 10% fetal bovine serum and kept at 37 °C in 5% CO_2. Transfection was conducted on the second day with

Lipofectamine 2000, when the cells reached ~70% confluence. A total of 2.5 μg of DNA was prepared for each well, containing the NEMO plasmid of interest together with an enhanced green fluorescent protein (EGFP) expression plasmid[36] and a tumor necrosis factor receptor 1 (TNFR1) plasmid, with the different amount of each vector listed in Table 1.

Table 1. Vectors Utilized (μg) in the Transfection of HEK293 Cells

vector	#1	#2	#3	#4	#5	#6
EGFP	0.1	0.1	0.1	0.1	0.1	0.1
TNFR1	0	0	0.1	0.1	0.1	0.1
NEMOwCcc	0	0.8	0	0.2	0.8	2.0
pcDNA3.1	2.4	1.4	2.3	2.1	1.5	0.3

The DNA/Lipofectamine 2000 mixture was prepared according to the Lipofectamine 2000 protocol (Invitrogen, Protocol Publication MAN0007824, revision 1.0), and a final volume of 250 μL of a mixture with 2.5 μg of DNA and 13.5 μL of Lipofectamine 2000 was added to each well.

After 48 h, cells were washed three times with 1× PBS and lysed in 250 μL of lysis buffer [50 mM HEPES (pH 7.3), 150 mM NaCl, 0.5% NP40, 2 mM EDTA, 10% glycerol, 0.1 mM Na_3VO_4, 1 mM PMSF, and one tablet of Roche protease inhibitor per 50 mL of buffer]. The total protein concentration in cell lysate was determined using the BCA assay (Pierce catalog no. 23225), so that for each sample the same amount of protein was used for Co-IP; 200 μg of lysate from each sample was treated with 30 μL of prewashed anti-FLAG M2 antibody conjugated to magnetic beads (Sigma), for a total volume of 400 μL, by addition of TBST [20 mM Tris (pH 7.5), 137 mM NaCl, and 0.5% Tween 20]. After incubation for 2 h at room temperature, the beads were washed three times with TBST buffer and boiled in 30 μL of urea–SDS buffer with DTT. The supernatant was separated from the beads by a magnetic rack and utilized for Western Blot analysis (separation by SDS–PAGE). NEMOwCcc was detected using the anti-FLAG M2 HRP-conjugated antibody (Sigma), while IKKβ was detected using anti-IKKβ (Cell Signaling) as a primary antibody and an anti-rabbit HRP-conjugated secondary antibody (Promega W401B). β-Actin was used as a control for the amount of lysate applied to the beads.

RESULTS

A schematic representation of all protein constructs examined here is given in Figure S1 of the Supporting Information. The sequences of the engineered NEMO constructs are listed in Table 2. For the sake of simplicity, we always refer to residues 44–111, although construct length differs slightly (see Table 2). The ideal coiled-coil sequence was chosen as designed by Havranek and Harbury and previously utilized to enforce Hsp90 N-domain proximity.[21,22] The heptad repeats of the modified GCN4 coiled coil were matched to the heptads in the sequence of NEMO(44–111) to select the insertion point. The cloning results were confirmed by DNA sequencing (MCB Core, Dartmouth College). All NEMO constructs express at high levels in *Escherichia coli* and are soluble in Tris buffer at pH 8. As previously reported,[20] because of their elongated structure, purified NEMO constructs have short retention times on SEC, corresponding approximately to a 44 kDa molecular mass marker, with the double coiled-coil construct being slightly larger than the others. NEMOw serves as our reference protein for comparison to all of the new constructs.

Enhanced Structure and Stability of Engineered NEMOs. SDS–PAGE, conducted under nonreducing conditions, shows that the coiled-coil constructs, like wild-type NEMO, exist in solution as covalently linked dimers (Figure 2). The introduction of the coiled-coil adaptor increases the dimer stability to progressively harsher conditions, including the presence of a reducing agent and sample heating to 95 °C. When compared to the NEMO(44–111) construct, the coiled-coil NEMO proteins display an α-helical content that increases from 54% for NEMOw to 70, 72, and 83% (Figure 3A,B), for NEMOwNcc, NEMOwCcc, and NEMOwDcc, respectively, as evidenced by the two characteristic minima at 208 and 222 nm in the CD spectra and predicted by the K2D3 method.[27,28] α-Helices in a coiled-coil conformation are characterized by greater ellipticity values at 222 nm than at 208 nm.[37,38] The 222 nm/208 nm intensity ratio indicates an increase in the level of coiled-coil structure in the designed constructs compared to that in wild-type NEMOw (Figure 3B). Thermal denaturation

Table 2. Sequences of the NEMO Constructs Examined[a]

Constructs	Sequences
NEMO(44-111)	GSEQGAPETLQRCLEENQELRDAIRQSNQILRERCEELLHFQASQREEKEFLMCKF QEARKLVERLGLEKLE
NEMOw	GSWEQGAPETLQRCLEENQELRDAIRQSNQILRERCEELLHFQASQREEKEFLMCK FQEARKLVERLGLEKLE
NEMOwNcc	GSWSVKELEDKNEELLSEIAHLKNEVARLKKLLQRCLEENQELRDAIRQSNQILRE RCEELLHFQASQREEKEFLMCKFQEARKLVERLGLEKLE
NEMOwCcc	GSWEQGAPETLQRCLEENQELRDAIRQSNQILRERCEELLHFQASQREEKEFLMCK FQEARKLVERLGLEKLELEDKNEELLSEIAHLKNEVARLKKLVGER
NEMOwDcc	GSWSVKELEDKNEELLSEIAHLKNEVARLKKLLQRCLEENQELRDAIRQSNQILRE RCEELLHFQASQREEKEFLMCKFQEARKLVERLGLEKLELEDKNEELLSEIAHLKN EVARLKKLVGER
NEMOwCcc8aa	GSWEQGAPETLQRCLEENQELRDAIRQSNQILRERCEELLHFQASQREEKEFLMCK FQEARKLVERLGLEKLELEDKNEEL

[a]The GS residues (gray) are appended after cleavage of the six-His tag. The W (blue) was inserted for ease of UV detection. The coiled-coil residues are colored orange. NEMO(44–111), NEMOw, and NEMOwCcc include NEMO residues 44–112 and the other constructs residues 51–112.

dx.doi.org/10.1021/bi500861x | *Biochemistry* 2014, 53, 6776–6785

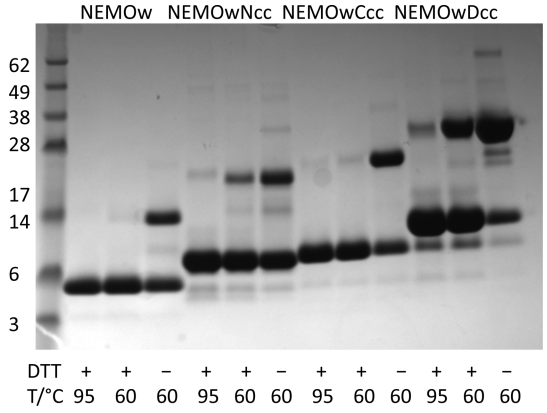

Figure 2. SDS−PAGE gel of the NEMO constructs as labeled: NEMOw, lanes 2−4; NEMOwNcc, lanes 5−7; NEMOwCcc, lanes 8−10; NEMOwDcc, lanes 11−13. MW markers in lane 1 are labeled. The heating temperature used in the preparation of the sample for electrophoresis is indicated as well as the presence or absence of the reducing agent DTT. For each construct, the lower band represents the monomer (MW = 8.8, 11.4, 12.1, and 14.8 kDa) and the upper band the dimer (NEMO constructs run lower than the calculated MW respect to MW standards, under these conditions).

curves monitored by CD are displayed in panels C and D of Figure 3, and the melting temperatures are summarized in Table 3. The results show that while NEMOw melts at room temperature (well before 30 °C), NEMOwCcc and NEMOwDcc are significantly more stable with melting temperatures around 65 °C, and melting curves typical of coiled-coil structures.[39,40] The N-terminal coiled-coil construct shows a gradual loss of secondary structure. The shortest engineered construct, NEMOwCcc8aa, is instead very similar to NEMOw in its secondary structure with no increase in coiled-coil content but shows improvement in its thermal stability with a midpoint of approximately 50 °C. We examined each construct in complex with IKKβ(701−745) (Figure 3D): most constructs show a more sigmoidal melting curve and no major changes in melting temperature. By comparison, our reference, NEMOw, shows improved stability with a melting temperature of 35 °C. NEMOwDcc experiences only partial loss of secondary structure with an increase in temperature. The total secondary structure in the complex reflects the non-completely helical structure of IKKβ(701−745) and the partial occupancy of NEMO at the concentration examined (unbound IKKβ is disordered).

Coiled-Coil Adaptors Rescue IKKβ Binding Affinity. We initially tested the ability of our reporter peptide (5′FAM-IKK$\beta_{KK/RR}$) to bind NEMO(44−111) using SEC. The unique UV absorbance of the 5′FAM fluorescein at 495 nm allows detection of the shift of the elution peak of 5′FAM-IKK$\beta_{KK/RR}$ to the molecular weight of the complex, upon co-injection with

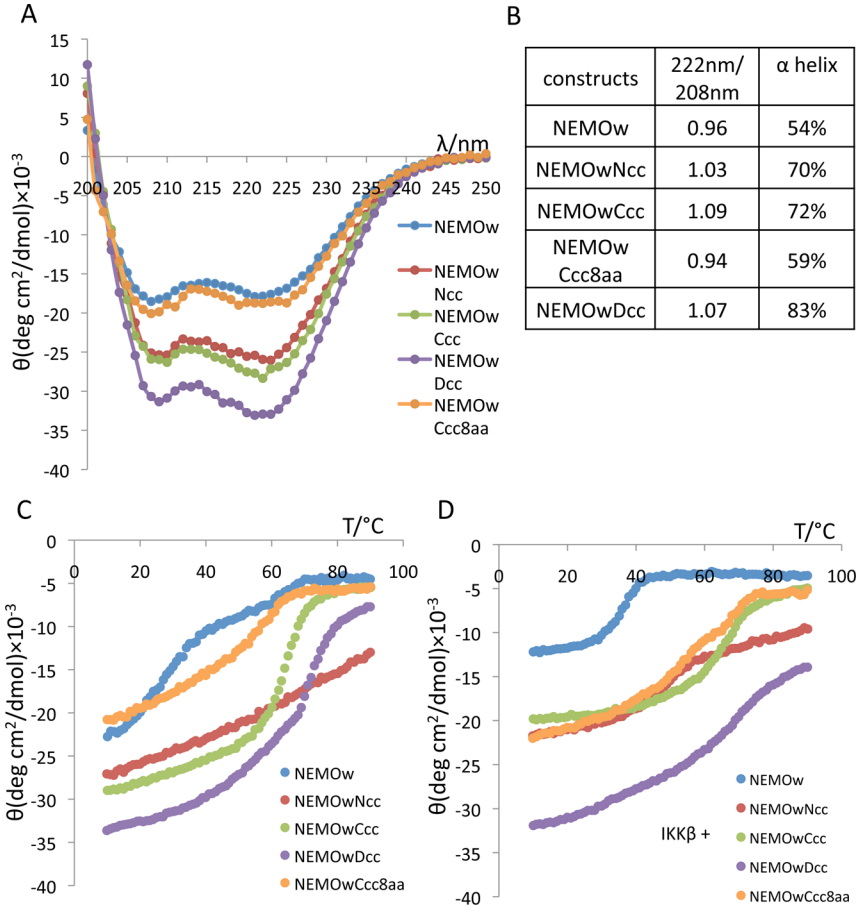

constructs	222nm/208nm	α helix
NEMOw	0.96	54%
NEMOwNcc	1.03	70%
NEMOwCcc	1.09	72%
NEMOw Ccc8aa	0.94	59%
NEMOwDcc	1.07	83%

Figure 3. (A) CD spectra of the NEMO constructs at 20 °C in Tris buffer (pH 8). (B) Plot of the 222 nm/208 nm intensity ratio. Values of >1 are indicative of coiled-coil structure, and the percent α-helix values were calculated by the K2D3 method. (C) CD melting curve of NEMO constructs, acquired between 10 and 90 °C, and monitored at 222 nm. (D) CD melting curve of NEMO constructs in the presence of IKKβ(701−745), at a 1:1 ratio.

dx.doi.org/10.1021/bi500861x | *Biochemistry* 2014, 53, 6776−6785

Table 3. Melting Temperatures (°C) of NEMOw and Engineered NEMO Constructs with and without IKKβ

	NEMOw	NEMOwNcc	NEMOwCcc	NEMOwDcc	NEMOwCcc8aa
alone	25	*a*	65	65−70	50−55
with IKKβ	35	45−50	65	60	50

[a]NEMOwNcc experiences a gradual decrease in secondary structure content as the temperature increases but does not display a sigmoidal melting curve with a defined midpoint.

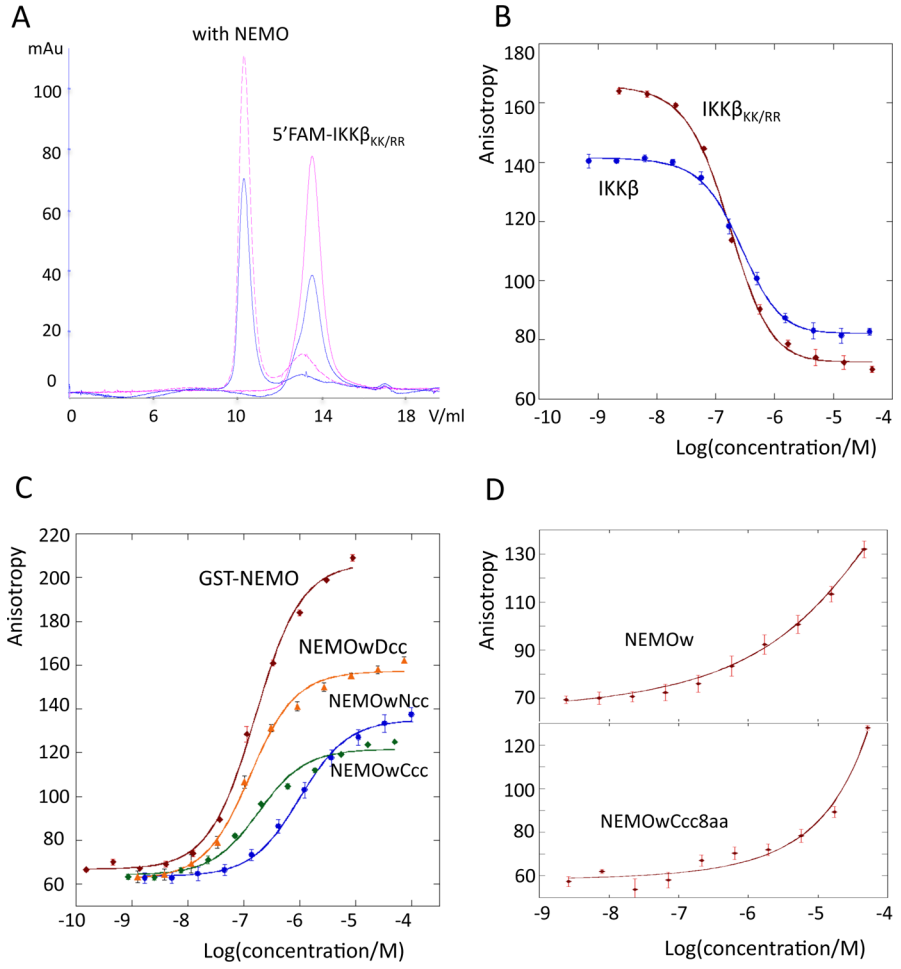

Figure 4. (A) SEC elution profile of 5′FAM-IKK$\beta_{KK/RR}$ with (···) and without NEMO. Data from monitoring at 280 nm are colored blue (total protein) and those at 495 nm red (IKKβ). The IKKβ absorption shifts to the complex molecular weight in the presence of NEMO. (B) IKKβ, IKK$\beta_{KK/RR}$ FA competition assay. (C) FA curves for direct binding of IKK$\beta_{KK/RR}$ to the engineered NEMO constructs and GST-NEMO(1−196). (D) FA direct binding of NEMOw and NEMOwCcc8aa. In panels B−D, the data represent the mean ± the standard deviation of three repeats.

Table 4. K_D Values Determined by Fluorescence Anisotropy, as Direct Binding of Fluorescent IKK$\beta_{KK/RR}$[a]

	NEMOwNcc	NEMOwCcc	NEMOwDcc	GST-NEMO(1−196)
K_D (nM)	980 ± 20	150 ± 6	114 ± 3	168 ± 4
		IKKβ		IKK$\beta_{KK/RR}$
IC_{50} (nM)		266 ± 13		167 ± 3

[a]IC_{50} values were determined by competition with fluorescent IKK$\beta_{KK/RR}$. NEMOw and NEMOwCcc8aa have K_D values of >1 μM. At the protein concentration tested, no complete binding curve was achieved, and the curves were therefore not fitted for K_D determination.

NEMOw (Figure 4A). We measured the affinity of the interaction by fluorescence anisotropy. The results are listed in Table 4 and Figure 4B−D. In the absence of the coiled-coil adaptor, NEMOw has a weak binding affinity (an approximate K_D of 10 μM can be qualitatively estimated from the incomplete binding curve). The addition of the N-terminal coiled coil in NEMOwNcc improves the affinity to <1 μM (980 ± 20 nM), and the C terminal coiled coil in NEMOwCcc (150 ± 6 nM) restores binding to the level of our control GST-NEMO(1−196) (168 ± 4 nM). With both ends zipped up by coiled coils, NEMOwDcc has an affinity of 114 ± 3 nM. In contrast, the short coiled-coil construct, NEMOwCcc8aa, behaves like NEMOw, and the binding curve does not reach a plateau at the maximal protein concentration tested, 52 μM.

NEMOwCcc8aa Folds Like Wild-Type NEMO upon Binding IKKβ. We further tested the ability of the coiled-coil-

dx.doi.org/10.1021/bi500861x | *Biochemistry* 2014, 53, 6776−6785

containing NEMO constructs to bind IKKβ(701−745) and produce a wild-type-like complex by NMR. ^{15}N-labeled NEMO(44−111) when binding IKKβ(701−745) produces a characteristic ^{1}H−^{15}N correlation spectrum. When NEMOwCcc8aa binds IKKβ(701−745), it reproduces the same dispersed pattern in a TROSY spectrum, with a few additional peaks arising from the appended coiled coil, indicating it assumes the same conformation when bound to IKKβ(701−745) (Figure 5).

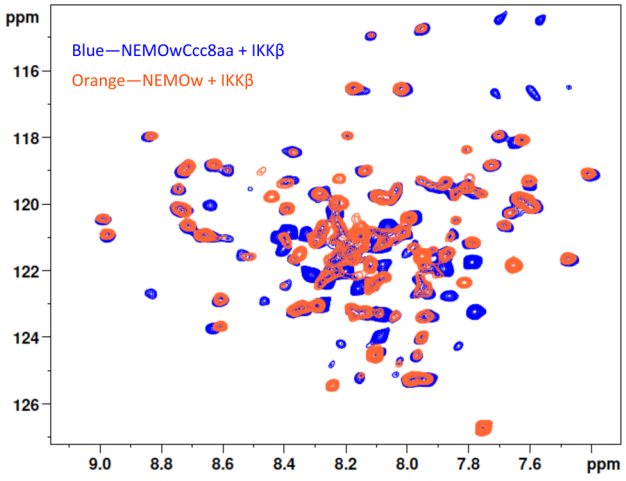

Figure 5. ^{1}H−^{15}N TROSY spectra of NEMOw (orange) and NEMOwCcc8aa (blue) in complex with IKKβ(701−745). Cross-peaks distinctive of the NEMO-bound conformation (e.g., region of 8.5−9.5 ppm) overlap in the two spectra, indicating the two NEMO constructs adopt the same conformation when bound to IKKβ. Additional peaks in the NEMOwCcc8aa spectrum are likely originating from the coiled-coil adaptor.

NEMOwCcc Recognizes Endogenous IKKβ in Mammalian Cells. To complement the *in vitro* binding assays, we tested a representative coiled-coil construct in mammalian cells and monitored its ability to interact with endogenous IKKβ. As shown in Figure 6 (compare lanes 1 and 2), only in the HEK293 cells transfected with FLAG-NEMOwCcc, when NEMOwCcc is captured using magnetic anti-FLAG antibody-conjugated beads, is IKKβ detected in the immunoprecipitate. In the control experiment, in the absence of transfected FLAG-NEMOwCcc, there is no detectable IKKβ. In lanes 3−6, an increase in the amount of FLAG-NEMOwCcc transfected in the cells causes a dose-dependent Co-IP of IKKβ, confirming that our engineered NEMO construct retains the ability to bind endogenous IKKβ in mammalian cells.

DISCUSSION

Our early description of the structure of the minimal NEMO−IKKβ complex coupled with structure prediction for the NEMO sequence suggests that the N-terminus of NEMO may exist as a dimer with at least partial coiled-coil character.[20] Unfortunately, the construct that we previously engineered, NEMO(44−111), while crystallizing in the presence of IKKβ(701−745), is not suitable for biophysical characterization or structural determination in its unbound form.[20] In this study, we set out to test if the addition of an ideal coiled-coil sequence, in one or four heptads, would be sufficient to nucleate structure in the NEMO(44−111) sequence, improve thermal stability, and restore binding affinity for IKKβ to the

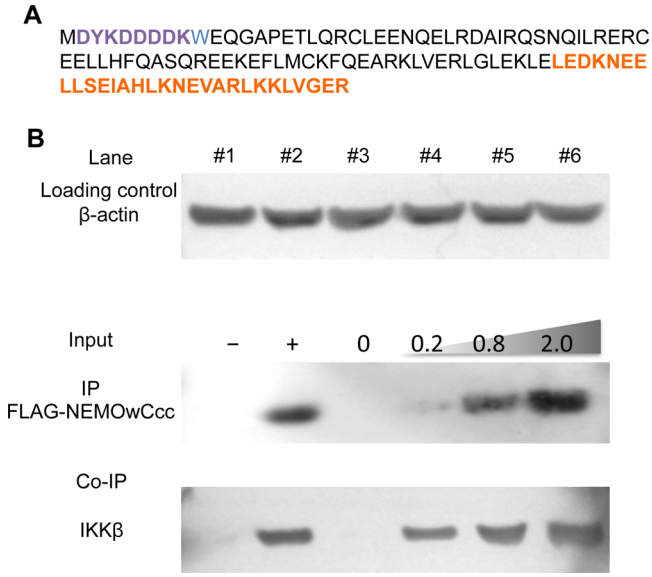

Figure 6. NEMOwCcc binds endogenous IKKβ in HEK293 cells. (A) Amino acid sequence of the FLAG-NEMOwCcc construct used in the co-immunoprecipitation (Co-IP) experiments. The FLAG tag is colored purple and the coiled-coil adaptor region orange. (B) HEK293 cells were transformed with (+) and without (−) FLAG-NEMOwCcc (lines 1 and 2) or with an increasing amount of input FLAG-NEMOwCcc (lines 3−6, amount indicated, in micrograms). Whole cell lysates were immunoprecipitated with anti-FLAG M2 beads, separated by SDS−PAGE, and immunoblotted for FLAG-NEMOwCcc and IKKβ. β-Actin was used as a loading control.

level of the longer constructs [e.g., NEMO(1−196)]. The coiled-coil motif has been extensively studied as a model system,[41,42] and the coiled-coil domain of the yeast transcription factor GCN4 has been specifically utilized to stabilize difficult proteins for structural studies (reviewed in ref 43). The crystal structures of 45 fusion proteins containing GCN4 adaptors, of which 14 are dimers, have been reported.[43] We chose a modified GCN4 sequence that was designed as a homodimeric coiled coil and was tested to be effective in inducing N-terminal proximity in Hsp90.[21,22] We incorporated repeats of the ideal coiled coil up to 29 residues long at either end or both ends of our construct, truncating a few residues from either the N- or C-terminal end to match the register of the predicted heptad repeats for the NEMO sequence. It has been shown that a good match of the fusion and insert portions maintaining a continuous heptad register generates a continuous seamless coil.[43]

Our results show that the engineered coiled-coil NEMO constructs exist as dimers, they preserve Cys-54 responsible for dimerization,[25] and dimer stability is enhanced by the presence of the coiled coils as demonstrated by SDS−PAGE. Stability to thermal denaturation is also improved, as monitored by CD and in fulfillment of one of the goals of the construct design. The results from CD additionally report on the secondary structure content of the proteins. NEMOw is characterized by a low percentage of α-helix (Figure 3B), indicative of a partially disordered structure and in agreement with what has been reported previously.[20] The insertion of a single heptad of the ideal coiled-coil sequence in NEMOwCcc8aa maintains a very similar structure, while insertion of a longer coiled-coil segment, corresponding to approximately four heptads, causes an increase in helical content in NEMOwNcc and NEM-

dx.doi.org/10.1021/bi500861x | *Biochemistry* 2014, 53, 6776−6785

OwCcc, with >80% helix in NEMOwDcc. These results imply not only that the ideal coiled-coil portion maintains its helical structure but also that the structure is propagated to the NEMO sequence "insert". On the basis of the 222 nm/208 nm ratio from CD spectra, all three engineered constructs with long coiled-coil attachments possess more coiled-coil structure than the parent NEMOw, which fulfills our additional aim to minimize the structural heterogeneity of apo NEMO. All coiled-coil constructs are also more stable to thermal denaturation, with a melting temperature reaching 65 °C for NEMOwDcc, and melting curves typical of coiled-coil structures (Figure 3C).

NEMOwNcc interestingly shows a progressive loss of secondary structure rather than a sigmoidal melting curve, which can be attributed to helix unraveling at either end of the structure. It is possible that the coiled coil at the N-terminus alters the original NEMO dimer packing pattern. According to secondary structure prediction, the first 40 amino acids of NEMO are predominantly disordered followed by a strong coiled-coil propensity up to residue 196 (Figure S2 of the Supporting Information). Enforcing a tightly zipped coiled coil at the N-terminus may induce a non-native fold in NEMO, not as well tolerated as a C-terminal coiled coil. All constructs maintain or improve thermal stability upon binding IKKβ (Figure 3D). In particular, the addition of coil zipping at both ends of NEMO(44−111) creates such a stable construct that upon binding of IKKβ the complex only slowly and partially unfolds at temperatures up to 90 °C (Figure 3D). NEMOwCcc8aa was designed after we observed the improved stability of NEMOwCcc, to test if a single heptad, when coupled with the native NEMO sequence, would create a sufficiently long segment with coiled-coil forming propensity to fold independently. Although it has been suggested that at least three heptad repeats are required to form a stable coiled coil, the engineered heptad fused to NEMO's native sequence imparts improved thermal stability to the construct. The coiled-coil character is indeed lower than those of the longer constructs.

One of the metrics we established for a successful engineered NEMO construct is an improvement in binding affinity for IKKβ, as an indication of nativelike behavior. In our hands, synthetically produced IKKβ(701−745) never retained the complete ability to bind NEMO [i.e., a population of unbound IKKβ was always observed even in the presence of a large excess of NEMO, both by NMR spectroscopy and by the SEC assay (data not shown)]. These observations dictated our use of a recombinantly produced IKKβ(701−745) in our FA assay. The only two lysines, close to the N-terminus of the protein, were mutated to arginines to prevent multisite labeling. On the basis of the direct binding and competition assays, the 5′-FAM-IKK$\beta_{KK/RR}$ binds to NEMO(1−196) like wild-type IKKβ(701−745) and represents a suitable probe for FA assays: a K_D of 168 ± 4 nM for binding of 5′-FAM-IKK$\beta_{KK/RR}$ to GST-NEMO(1−196) was obtained. In homologous, IKK$\beta_{KK/RR}$, and heterologous, IKKβ(701−745), competition assays, IC_{50} values of 167 and 266 nM were obtained, respectively. These results are in accord with literature values, which range from low micromolar values to low nanomolar values, depending on the method utilized.[20,44,45]

Our FA results show improved affinity for all three engineered constructs. Unfortunately, NEMOw, used as a baseline, starts aggregating at elevated concentrations, and therefore, an accurate K_D cannot be obtained, with an estimated value in the low micromolar range. NEMOwNcc has the weakest affinity of 980 ± 20 nM, in agreement with the discussed poor structural match of an N-terminal coiled coil to wild-type NEMO. Meanwhile, NEMOwCcc and NEMOwDcc show affinities of 150 ± 6 and 114 ± 3 nM, the same level as observed for GST-NEMO(1−196). Together with the thermal stability results, it is clear that via fusion of a coiled-coil sequence at the C-terminus, the short NEMO construct can be stabilized and its IKKβ binding ability can be restored to the level of NEMO(1−196).

$^{1}H-^{15}N$ HSQC NMR spectroscopy is widely employed to monitor protein folding characteristics and solution behavior, and the spectra are often termed the "fingerprint" of the protein for their sensitivity to any change in conformation, environment, or interaction. Indeed, HSQC spectra are some of the most diffused tools in NMR-based screening to monitor protein binding to even very low affinity ligands.[46] We have utilized the $^{1}H-^{15}N$ TROSY spectrum (which provides $^{1}H-^{15}N$ correlations as the HSQC but gave us better results for a complex of the size and shape of the NEMO−IKKβ complex) to monitor the effect of binding of unlabeled IKKβ to [^{15}N]NEMOw and [^{15}N]NEMOwCcc8aa. If NEMOw and NEMOwCcc8aa bind IKKβ in the same manner, they will produce a similar spectral pattern (same residues resonating at the same frequencies), while if the coiled-coil extension produced a non-native binding for NEMOwCcc8aa, the spectra would be different. The spectrum of NEMOwCcc8aa bound to IKKβ(701−745) displays a pattern very similar to the spectrum of our reference NEMOw under the same conditions, indicating that upon binding to IKKβ(701−745), residues from the wild-type and engineered NEMO constructs experience the same interactions, and the coiled-coil adaptor does not alter the folding of NEMO.

Our NEMOwCcc construct best fulfills the requirements of stability, size, structural content and homogeneity, and nativelike binding affinity for the NEMO-binding domain of IKKβ. NEMOwCcc also retains the ability to bind endogenous IKKβ in mammalian cells, and Co-IP of IKKβ shows a dependence of the dose on the amount of FLAG-NEMOwCcc transfected. The experiment further confirms that NEMOwCcc is a good mimetic for the IKK-binding domain in NEMO and represents a nontrivial improvement over our original construct of NEMO(44−111).[20]

CONCLUSIONS

A C-terminal fusion with approximately four heptads of an ideal coiled-coil sequence based on GCN4 successfully stabilized the short NEMO(44−111) construct. The original NEMO(44−111) is characterized by structural heterogeneity and is marginally stable at room temperature, while our best engineered construct is thermally stable with an improvement of ∼40 °C in melting temperature. The homodimeric coiled-coil design also rescues IKKβ binding affinity to the level of GST-NEMO(1−196), suggesting that the IKK-binding domain of NEMO may exist as a stable coiled-coil dimer within the native protein and the conformational heterogeneity of NEMO(44−111) is an artifact of protein truncation rather than a requirement for IKKβ binding. The stabilization induced by the coiled-coil fusion may additionally favor structural studies aimed at the determination of the structure of unliganded NEMO, of NEMO bound to small peptides and/or molecules (e.g., the NBD peptide), and future screening efforts to identify small molecule inhibitors.

dx.doi.org/10.1021/bi500861x | Biochemistry 2014, 53, 6776−6785

■ ASSOCIATED CONTENT

Supporting Information

All the primers and protein constructs (Supplementary Table 1 and Figure 1) and coiled-coil prediction of the NEMO(1−196) construct (Supplementary Figure 2). This material is available free of charge via the Internet at http://pubs.acs.org.

■ AUTHOR INFORMATION

Corresponding Author

*Dartmouth College, 6128 Burke Hall, Hanover, NH 03755. Telephone: (603) 646-8103. Fax: (603) 646-3946. E-mail: maria.pellegrini@dartmouth.edu.

Funding

Research reported in this publication was supported by the National Institute of Arthritis and Musculoskeletal and Skin Diseases of the National Institutes of Health via Grant R03AR066130.

Notes

The authors declare no competing financial interest.

■ ACKNOWLEDGMENTS

M.P. thanks Prof. D. Bolon (University of Massachusetts Medical School) for the kind gift of the plasmid containing the optimized GCN4 coiled coil and Dr. P. Schneider (University of Lausanne, Lausanne, Switzerland) for his advice and the gift of plasmids for the mammalian cell experiments. The work was executed in the Department of Chemistry of Dartmouth College.

■ REFERENCES

(1) Jin, D. Y., and Jeang, K. T. (1999) Isolation of full-length cDNA and chromosomal localization of human NF-κB modulator NEMO to Xq28. *J. Biomed. Sci. 6*, 115−120.

(2) Karin, M., Cao, Y., Greten, F. R., and Li, Z.-W. (2002) NF-κB in cancer: From innocent bystander to major culprit. *Nat. Rev. Cancer 2*, 301−310.

(3) Hoffmann, A., Natoli, G., and Ghosh, G. (2006) Transcriptional regulation via the NF-κB signaling module. *Oncogene 25*, 6706−6716.

(4) Israel, A. (2010) The IKK Complex, a Central Regulator of NF-κB Activation. *Cold Spring Harbor Perspect. Biol. 2*, a000158.

(5) Gilmore, T. D., and Herscovitch, M. (2006) Inhibitors of NF-κB signaling: 785 and counting. *Oncogene 25*, 6887−6899.

(6) Gasparini, C., and Feldmann, M. (2012) NF-κB as a target for modulating inflammatory responses. *Curr. Pharm. Des. 18*, 5735−5745.

(7) Chen, Z., Hagler, J., Palombella, V. J., Melandri, F., Scherer, D., Ballard, D., and Maniatis, T. (1995) Signal-induced site-specific phosphorylation targets IκBα to the ubiquitin-proteasome pathway. *Genes Dev. 9*, 1586−1597.

(8) Palombella, V. J., Rando, O. J., Goldberg, A. L., and Maniatis, T. (1994) The ubiquitin-proteasome pathway is required for processing the NF-κB1 precursor protein and the activation of NF-κB. *Cell 78*, 773−785.

(9) DiDonato, J. A., Mercurio, F., and Karin, M. (2012) NF-κB and the link between inflammation and cancer. *Immunol. Rev. 246*, 379−400.

(10) Whitty, A., and Kumaravel, G. (2006) Between a rock and a hard place? *Nat. Chem. Biol. 2*, 112−118.

(11) Smith, M. C., and Gestwicki, J. E. (2012) Features of protein-protein interactions that translate into potent inhibitors: Topology, surface area and affinity. *Expert Rev. Mol. Med. 14*, e16.

(12) Solt, L. A., Madge, L. A., and May, M. J. (2009) NEMO-binding domains of both IKKα and IKKβ regulate IκB kinase complex assembly and classical NF-κB activation. *J. Biol. Chem. 284*, 27596−27608.

(13) May, M. J., D'Acquisto, F., Madge, L. A., Glöckner, J., Pober, J. S., and Ghosh, S. (2000) Selective Inhibition of NF-κB Activation by a Peptide That Blocks the Interaction of NEMO with the IκB Kinase Complex. *Science 289*, 1550−1554.

(14) Habineza Ndikuyeze, G., Gaurnier-Hausser, A., Patel, R., Baldwin, A. S., May, M. J., Flood, P., Krick, E., Propert, K. J., and Mason, N. J. (2014) A Phase I Clinical Trial of Systemically Delivered NEMO Binding Domain Peptide in Dogs with Spontaneous Activated B-Cell like Diffuse Large B-Cell Lymphoma. *PLoS One 9*, e95404.

(15) Tanaka, T., Nakayama, H., Yoshitake, Y., Irie, A., Nagata, M., Kawahara, K., Takamune, Y., Yoshida, R., Nakagawa, Y., Ogi, H., Shinriki, S., Ota, K., Hiraki, A., Ikebe, T., Nishimura, Y., and Shinohara, M. (2012) Selective inhibition of nuclear factor-κB by nuclear factor-κB essential modulator-binding domain peptide suppresses the metastasis of highly metastatic oral squamous cell carcinoma. *Cancer Sci. 103*, 455−463.

(16) Acharyya, S., Villalta, S. A., Bakkar, N., Bupha-Intr, T., Janssen, P. M., Carathers, M., Li, Z. W., Beg, A. A., Ghosh, S., Sahenk, Z., Weinstein, M., Gardner, K. L., Rafael-Fortney, J. A., Karin, M., Tidball, J. G., Baldwin, A. S., and Guttridge, D. C. (2007) Interplay of IKK/NF-κB signaling in macrophages and myofibers promotes muscle degeneration in Duchenne muscular dystrophy. *J. Clin. Invest. 117*, 889−901.

(17) Dai, Y., Chen, S., Wang, L., Pei, X.-Y., Funk, V. L., Kramer, L. B., Dent, P., and Grant, S. (2011) Disruption of IκB kinase (IKK)-mediated RelA serine 536 phosphorylation sensitizes human multiple myeloma cells to histone deacetylase (HDAC) inhibitors. *J. Biol. Chem. 286*, 34036−34050.

(18) Delfín, D. A., Xu, Y., Peterson, J. M., Guttridge, D. C., Rafael-Fortney, J. A., and Janssen, P. M. (2011) Improvement of cardiac contractile function by peptide-based inhibition of NF-κB in the utrophin/dystrophin-deficient murine model of muscular dystrophy. *J. Transl. Med. 9*, 68.

(19) Ianaro, A., Tersigni, M., Belardo, G., Martino, S. D., Napolitano, M., Palmieri, G., Sini, M., Maio, A. D., Ombra, M., Gentilcore, G., Capone, M., Ascierto, M., Satriano, R. A., Farina, B., Faraone-Mennella, M., Ascierto, P. A., and Ialenti, A. (2009) NEMO-binding domain peptide inhibits proliferation of human melanoma cells. *Cancer Lett. 274*, 331−336.

(20) Rushe, M., Silvian, L., Bixler, S., Chen, L. L., Cheung, A., Bowes, S., Cuervo, H., Berkowitz, S., Zheng, T., Guckian, K., Pellegrini, M., and Lugovskoy, A. (2008) Structure of a NEMO/IKK-Associating Domain Reveals Architecture of the Interaction Site. *Structure 16*, 798−808.

(21) Havranek, J. J., and Harbury, P. B. (2003) Automated design of specificity in molecular recognition. *Nat. Struct. Biol. 10*, 45−52.

(22) Pullen, L., and Bolon, D. N. (2011) Enforced N-domain proximity stimulates Hsp90 ATPase activity and is compatible with function in vivo. *J. Biol. Chem. 286*, 11091−11098.

(23) Audu, C. O., Cochran, J. C., Pellegrini, M., and Mierke, D. F. (2013) Recombinant production of TEV cleaved human parathyroid hormone. *J. Pept. Sci. 19*, 504−510.

(24) Gasteiger, E., Hoogland, C., Gattiker, A., Duvaud, S., Wilkins, M. R., Appel, R. D., and Bairoch, A. (2005) Protein Identification and Analysis Tools on the ExPASy Server. In *The Proteomics Protocols Handbook* (Walker, J. M., Ed.) pp 571−607, Humana Press, Totowa, NJ.

(25) Cote, S. M., Gilmore, T. D., Shaffer, R., Weber, U., Bollam, R., Golden, M. S., Glover, K., Herscovitch, M., Ennis, T., Allen, K. N., and Whitty, A. (2013) Mutation of nonessential cysteines shows that the NF-κB essential modulator forms a constitutive noncovalent dimer that binds IκB kinase-β with high affinity. *Biochemistry 52*, 9141−9154.

(26) Myers, J. K., Pace, C. N., and Scholtz, J. M. (1997) Helix propensities are identical in proteins and peptides. *Biochemistry 36*, 10923−10929.

(27) Holzwarth, G., and Doty, P. (1965) The ultraviolet circular dichroism of polypeptides. *J. Am. Chem. Soc. 87*, 218−228.

(28) Louis-Jeune, C., Andrade-Navarro, M. A., and Perez-Iratxeta, C. (2012) Prediction of protein secondary structure from circular dichroism using theoretically derived spectra. *Proteins 80*, 374−381.
(29) Cushing, P. R., Fellows, A., Villone, D., Boisguérin, P., and Madden, D. R. (2008) The relative binding affinities of PDZ partners for CFTR: A biochemical basis for efficient endocytic recycling. *Biochemistry 47*, 10084−10098.
(30) *Principles of Fluorescence Spectroscopy*. 2006, (Lakowicz, J. R., Ed.) Springer US.
(31) Swillens, S. (1995) Interpretation of binding curves obtained with high receptor concentrations: Practical aid for computer analysis. *Mol. Pharmacol. 47*, 1197−1203.
(32) Lazareno, S., and Birdsall, N. J. (1993) Estimation of competitive antagonist affinity from functional inhibition curves using the Gaddum, Schild and Cheng-Prusoff equations. *Br. J. Pharmacol. 109*, 1110−1119.
(33) Czisch, M., and Boelens, R. (1998) Sensitivity enhancement in the TROSY experiment. *J. Magn. Reson. 134*, 158−160.
(34) Pervushin, K. V., Wider, G., and Wüthrich, K. (1998) Single Transition-to-single Transition Polarization Transfer (ST2-PT) in [^{15}N,^{1}H]-TROSY. *J. Biomol. NMR 12*, 345−348.
(35) Grzesiek, S., and Bax, A. (1993) The importance of not saturating water in protein NMR. Application to sensitivity enhancement and NOE measurements. *J. Am. Chem. Soc. 115*, 12593−12594.
(36) Schneider, P. (2000) Production of recombinant TRAIL and TRAIL receptor: Fc chimeric proteins. *Methods Enzymol. 322*, 325−345.
(37) Cooper, T. M., and Woody, R. W. (1990) The effect of conformation on the CD of interacting helices: A theoretical study of tropomyosin. *Biopolymers 30*, 657−676.
(38) Greenfield, N. J., and Hitchcock-Degregori, S. E. (1993) Conformational intermediates in the folding of a coiled-coil model peptide of the N-terminus of tropomyosin and $\alpha\alpha$-tropomyosin. *Protein Sci. 2*, 1263−1273.
(39) Thomas, F., Boyle, A. L., Burton, A. J., and Woolfson, D. N. (2013) A Set of de Novo Designed Parallel Heterodimeric Coiled Coils with Quantified Dissociation Constants in the Micromolar to Sub-nanomolar Regime. *J. Am. Chem. Soc. 135*, 5161−5166.
(40) Barth, P., Schoeffler, A., and Alber, T. (2008) Targeting Metastable Coiled-Coil Domains by Computational Design. *J. Am. Chem. Soc. 130*, 12038−12044.
(41) Lupas, A., Van Dyke, M., and Stock, J. (1991) Predicting coiled coils from protein sequences. *Science 252*, 1162−1164.
(42) Lupas, A. N., and Gruber, M. (2005) The structure of α-helical coiled coils. *Adv. Protein Chem. 70*, 37−78.
(43) Deiss, S., Hernandez Alvarez, B., Bär, K., Ewers, C. P., Coles, M., Albrecht, R., and Hartmann, M. D. (2014) Your personalized protein structure: Andrei N. Lupas fused to GCN4 adaptors. *J. Struct. Biol. 186*, 380−385.
(44) Lo, Y.-C., Maddineni, U., Chung, J. Y., Rich, R. L., Myszka, D. G., and Wu, H. (2008) High-Affinity Interaction between IKKβ and NEMO. *Biochemistry 47*, 3109−3116.
(45) Baima, E. T., Guzova, J. A., Mathialagan, S., Nagiec, E. E., Hardy, M. M., Song, L. R., Bonar, S. L., Weinberg, R. A., Selness, S. R., Woodard, S. S., Chrencik, J., Hood, W. F., Schindler, J. F., Kishore, N., and Mbalaviele, G. (2010) Novel Insights into the Cellular Mechanisms of the Anti-inflammatory Effects of NF-κB Essential Modulator Binding Domain Peptides. *J. Biol. Chem. 285*, 13498−13506.
(46) Shuker, S. B., Hajduk, P. J., Meadows, R. P., and Fesik, S. W. (1996) Discovering high-affinity ligands for proteins: SAR by NMR. *Science 274*, 1531−1534.